Earth and Planetary Science Letters 404 (2014) 14–21

Contents lists available at ScienceDirect

Earth and Planetary Science Letters

www.elsevier.com/locate/epsl

Elastic properties of stishovite and the $CaCl_2$-type silica at the mantle temperature and pressure: An ab initio investigation

Rui Yang [a,b], Zhongqing Wu [a,b,*]

[a] Laboratory of Seismology and Physics of Earth's Interior, School of Earth and Space Sciences, University of Science and Technology of China, Hefei 230026, China
[b] National Geophysical Observatory at Mengcheng, Anhui, China

ARTICLE INFO

Article history:
Received 2 May 2014
Received in revised form 16 July 2014
Accepted 18 July 2014
Available online xxxx
Editor: J. Brodholt

Keywords:
elasticity
density functional theory calculations
phase transition of silica

ABSTRACT

The elastic constant tensors of stishovite and the $CaCl_2$-type silica at the Earth's mantle temperature and pressure were determined using first-principles calculations with local density approximation. The elastic properties of stishovite show not only strong pressure dependence but also temperature dependence. By increasing temperature, the shear instability of stishovite is shifted to an elevated pressure with a slope of $\sim 5.4 \pm 1.4$ MPa/K. The softening of the shear modulus and the positive Clapeyron slope result in crossing of the sound velocities at different temperatures, which leads to the unusual positive temperature dependence of the sound velocities around the phase boundary. The transition from stishovite to the $CaCl_2$-type silica at the lower mantle's temperature occurs at a depth far deeper than 1200 km and is accompanied by a velocity jump of $\sim 0.98 \pm 0.08$ km/s in S wave velocity (V_S) and $\sim 0.45 \pm 0.15$ km/s in P wave velocity (V_P). This transition is likely related to the seismic discontinuity at the depth of $\sim$1670 km in the vicinity of Mariana Island. The unusual positive temperature dependence of V_S of stishovite and strong anisotropy of stishovite and the $CaCl_2$-type silica around the phase boundary provide potential ways to identify the origin of the seismic discontinuity.

1. Introduction

The properties of stishovite and its high-pressure polymorph are of great interest in geophysics. The natural mid-oceanic ridge basalt (MORB) has 10–20% of free silica at the lower mantle condition (Irifune and Ringwood, 1993; Kesson et al., 1994; Ono et al., 2001). Stishovite is stable at $P > \sim 10$ GPa and known to go through a transformation to an orthorhombic $CaCl_2$-type structure at the lower mantle pressure. The transition has been extensively studied by both experiments and theoretical calculations (e.g. Andrault et al., 1998, 2003; Asahara et al., 2013; Belonoshko and Dubrovinsky, 1996; Carpenter, 2006; Carpenter et al., 2000; Cohen, 1991, 1992; Driver et al., 2010; Dubrovinsky and Belonoshko, 1996; Hemley et al., 2000; Karki et al., 1997a, 1997b; Kingma et al., 1995; Lee and Gonze, 1995, 1997; Ono et al., 2002; Shieh et al., 2002; Togo et al., 2008; Tsuchida and Yagi, 1989; Tsuchiya et al., 2004; Tsuneyuki et al., 1989; Zha et al., 1994). The elasticity of stishovite and the $CaCl_2$-type silica has been investigated by experiments at room temperature and high pressure (Jiang et al., 2009; Li et al., 1996; Shieh et al., 2002; Weidner et al., 1982) or at ambient pressure and high temperature (Brazhkin et al., 2005) as well as by first-principles calculations without including temperature effect (Cohen, 1991, 1992; Holm and Ahuja, 1999; Karki et al., 1997b; Tsuneyuki et al., 1989). The knowledge of the high-temperature and -pressure elasticity of stishovite and the $CaCl_2$-type silica, which is critical for us to understand Earth's interior, however, remains very limited.

Isothermal elastic constants are given by Barron and Klein (1965)

$$c^T_{ijkl} = \frac{1}{V}\left(\frac{\partial^2 F}{\partial e_{ij}\partial e_{kl}}\right) + \frac{1}{2}P(2\delta_{ij}\delta_{kl} - \delta_{il}\delta_{kj} - \delta_{ik}\delta_{jl}) \quad (1)$$

Here, e_{ij} ($i = 1$–3) are infinitesimal strains, and F is the Helmholtz free energy, which is expressed in the quasi-harmonic approximation as

$$F(e_{ij}, V, T) = U(e_{ij}, V) + \frac{1}{2}\sum_{q,m}\hbar\omega_{q,m}(e_{ij}, V) + k_B T \sum_{q,m} \ln\left\{1 - \exp\left[-\frac{\hbar\omega_{q,m}(e_{ij}, V)}{k_B T}\right]\right\}, \quad (2)$$

* Corresponding author at: Laboratory of Seismology and Physics of Earth's Interior, School of Earth and Space Sciences, University of Science and Technology of China, Hefei 230026, China.
E-mail address: wuzq10@ustc.edu.cn (Z. Wu).

http://dx.doi.org/10.1016/j.epsl.2014.07.020
0012-821X/

where ω is vibrational frequency, q is the phonon wave vector, m is the normal mode index. The first, second, and third terms are the static internal, zero point, and vibrational energy contributions at volume V under isotropic pressure, respectively. Calculations of the elastic tensors usually require free energy and hence vibrational density of states for many strained configurations (e.g. at least 15 strained configurations for orthorhombic crystal). Therefore, the computation of the elastic tensors at high-temperature and -pressure is considerably expensive. Wu and Wentzcovitch (2011) deduced an analytical formula for this second derivative and developed a method of calculating the elastic constants without requiring vibrational density of states for the strained configurations. The method reduces the computation time to less than ten percent of the usual method and has been applied successfully to MgO (Wu and Wentzcovitch, 2011), diamond (Núñez Valdez et al., 2012a), olivine and its polymorph (Núñez Valdez et al., 2012b, 2013), and ferropericlase (Wu et al., 2013). Here we applied the method to stishovite and the $CaCl_2$-type silica and obtained their high-temperature and -pressure elastic constant tensors.

2. Method

Calculations were performed using the open-source Quantum ESPRESSO package (Giannozzi et al., 2009) based on the density functional theory (DFT). The local density approximation (Kohn and Sham, 1965) was adopted for the exchange correlation function. A plane wave basis set with a 70 Ry cut-off energy was used to expand the valence wave functions at the special K-points generated by a $4 \times 4 \times 4$ mesh (Monkhorst and Pack, 1976) for both of the polymorphs of silica. The silicon and oxygen pseudopotential were generated by the norm-conserving Troullier–Martins (Troullier and Martins, 1991) method. The structure at certain pressure was optimized using the variable cell-shape damped molecular dynamic (Wentzcovitch et al., 1993). The dynamical matrices on a $4 \times 4 \times 4$ mesh for the optimized structure, computed using density functional perturbation theory (DFPT) (Baroni et al., 2001), were interpolated in a regular $7 \times 7 \times 9$ mesh to obtain the vibrational density of state. The static elastic constant tensors were calculated from stresses generated by small deformation of the optimized unit cell with internal atomic coordinated relaxation. The strain values $\pm 0.5\%$ and $\pm 1.0\%$ were chosen to calculate the stresses. The stresses and the strains show good linear relation and were fitted linearly to get the static elastic constant tensors. Then the Wu and Wentzcovitch (2011) method was used to obtain the high-temperature and -pressure elastic tensors.

Wu and Wentzcovitch (2011) obtained the basic knowledge on the strain dependence of phonon frequencies, which is needed at calculating elasticity at high temperature (see Eqs. (1)–(2)), from volume dependence of phonon frequencies after introducing an approximation. Volume dependence of phonon frequencies is described by mode Grüneisen parameters, while the strain dependence of phonon frequencies is described by strain Grüneisen parameters. The frequency change expressed by mode Grüneisen parameters

$$\frac{d\omega_{qm}}{\omega_{qm}} = -\gamma_{qm}\frac{dV}{V} \tag{3}$$

should be the same to the frequency change expressed by strain Grüneisen parameters

$$\frac{d\omega_{qm}}{\omega_{qm}} = -\left(\gamma_{qm}^{11}e_{11} + \gamma_{qm}^{22}e_{22} + \gamma_{qm}^{33}e_{33}\right). \tag{4}$$

Here e_{ii} $(i = 1\text{–}3)$ are non-zero infinitesimal strains along three axis of orthorhombic crystals under hydrostatic compression. Then we have

$$\begin{aligned}
\gamma_{qm}^{11} &= \frac{e_{11}+e_{22}+e_{33}}{e_{11}}\gamma_{qm}\cos^2\theta_{qm}\sin^2\phi_{qm} \\
\gamma_{qm}^{22} &= \frac{e_{11}+e_{22}+e_{33}}{e_{22}}\gamma_{qm}\sin^2\theta_{qm}\sin^2\phi_{qm} \\
\gamma_{qm}^{33} &= \frac{e_{11}+e_{22}+e_{33}}{e_{33}}\gamma_{qm}\cos^2\phi_{qm}
\end{aligned} \tag{5}$$

Here θ_{qm} and ϕ_{qm} are mode dependence parameters. A distribution function $f(\theta,\phi)$, defining the density of modes with θ_{qm} and ϕ_{qm} between (θ,ϕ) and $(\theta+d\theta,\phi+d\phi)$, is introduced. For isotropic materials $f(\theta,\phi)$ must be a constant. Wu and Wentzcovitch (2011) assumed this constant distribution for crystals and obtained an analytical formula for the second derivative of vibrational-related free energy with respect to the infinitesimal strains expressed by γ_{qm}, mode Grüneisen parameters. The anisotropy of crystal is embodied by e_{ii} under hydrostatic compression. Since mode Grüneisen parameters γ_{qm}, which describe the volume dependence of the frequencies, can be obtained from one phonon DoS calculation at each volume, the method reduces the computational effort i.e., CPU time and human labor, less than ten percent of the usual method. Furthermore, the results are indeed at infinitesimal strains since no strains are applied in practice. "Infinitesimal" strains in the usual method are small but non-vanishing, which is a compromise between a small strain and good numerical accuracy for energy differences between strained configurations. Successful applications of the method to various materials (Núñez Valdez et al., 2012a, 2012b, 2013; Wu and Wentzcovitch, 2011; Wu et al., 2013) indicate that the approximation introduced works well for different kind of crystals.

The Helmholtz free energies were calculated using the quasi-harmonic approximation with the static energy and vibrational density of state at volume V under isotropic pressure (Eq. (1)). The calculated Helmholtz free energies versus volume were fitted by isothermal third-order finite strain equations of state. Then all thermodynamic properties including Gibbs free energy can be derived from the Helmholtz free energies. The phase boundary between stishovite and $CaCl_2$-type silica was obtained by comparing their Gibbs free energies. Root mean square deviation of free energy was used to estimate the uncertainty of the transition pressure.

3. Results

3.1. The elastic properties

The elastic constants (C_{ij} with Voigt notation), six for the tetragonal structured stishovite and nine for the orthorhombic structured $CaCl_2$-type silica, are shown in Figs. 1 and 2 as a function of pressure at different temperatures. The calculated results for stishovite at 0 GPa and for the $CaCl_2$-type silica at 50 GPa agree well with available experiment reports and previous calculations (Table 1). Static results do not include the zero-motion contribution and 300 K temperature contribution to the elastic constants. Both of the effects can increase the equilibrium volume (see Fig. 3) and hence reduce the elastic constants. The difference between the static and 300K's elastic constants is noticeable for most of the elastic constants especially for C_{12}. In contrast to all the other elastic constants, C_{12} is the most sensitive to the volume variation.

As shown in Fig. 1, static C_{11} increases with pressure at low pressure and begins softening above ~40 GPa. In contrast to C_{11}, C_{12} increases rapidly with pressure and finally becomes larger

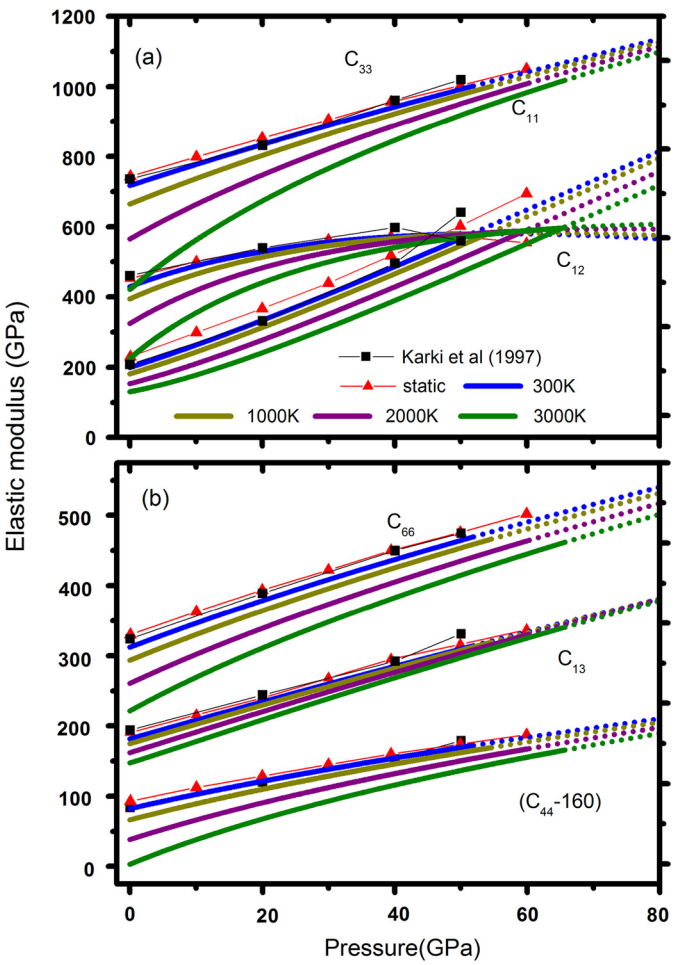

Fig. 1. Pressure dependence of elastic modulus of stishovite at different temperatures, (a) C_{11}, C_{12} and C_{33}, (b) C_{44}, C_{13} and C_{66}. Previous static calculation results reported by Karki et al. (1997b) are also listed. The results above the pressure of shear instability are shown in the dotted lines.

than C_{11} at ~46 GPa for the static result. Negative C_{11}–C_{12}, based on the Born criteria, indicates that stishovite is shear instable at $P > 46$ GPa. This shear instability of stishovite has been shown to be associated with the transition from the tetragonal phase to the orthorhombic $CaCl_2$ phase of SiO_2 (e.g. Andrault et al., 1998; Cohen, 1992; Karki et al., 1997b; Kingma et al., 1995; Togo et al., 2008). With increasing temperature, the shear instability is shifted to the elevated pressure (Fig. 4). The slope of the shear instability is 5.4 ± 1.4 MPa/K. The phase boundary between stishovite and $CaCl_2$-type silica based on Gibbs free energies is also shown in Fig. 4. The transition pressures from stishovite to $CaCl_2$-type silica based on Gibbs free energy are slight smaller than those based on the shear instability. The Clapeyron slope of the phase transition is 5.0 ± 1.3 MPa/K. Anharmonic effect ignored by quasi-harmonic approximation becomes important at high temperature and will affect the Clapeyron slope (Wu and Wentzcovitch, 2009; Wu, 2010). The previous calculations (Tsuchiya et al., 2004) considered this anharmonic effect to some extent and obtained Clapeyron slope 6.0 MPa/K. Therefore, we can expect that anharmonic effect ignored in this calculation should increase Clapeyron slope of the transition. The boundary of shear instability significantly overlaps with the phase boundary considering their large uncertainties. It is highly possible that the phase transition from stishovite to $CaCL_2$-type silica is triggered by shear instability of stishovite. C_{33} is far larger than C_{11} whatever the pressure and temperature are, indicating the difference of the compressibility along different axes. Most of the elastic constants of the $CaCl_2$-type silica increase monotonically with pressure except for C_{12} and C_{23} (Fig. 2). Non-monotonical pressure dependence of C_{12} and C_{23} leads to the complex temperature-dependence of C_{12} and C_{23}. Namely, C_{12} and C_{23} increase with temperature at some pressures while decrease with temperature at other pressures.

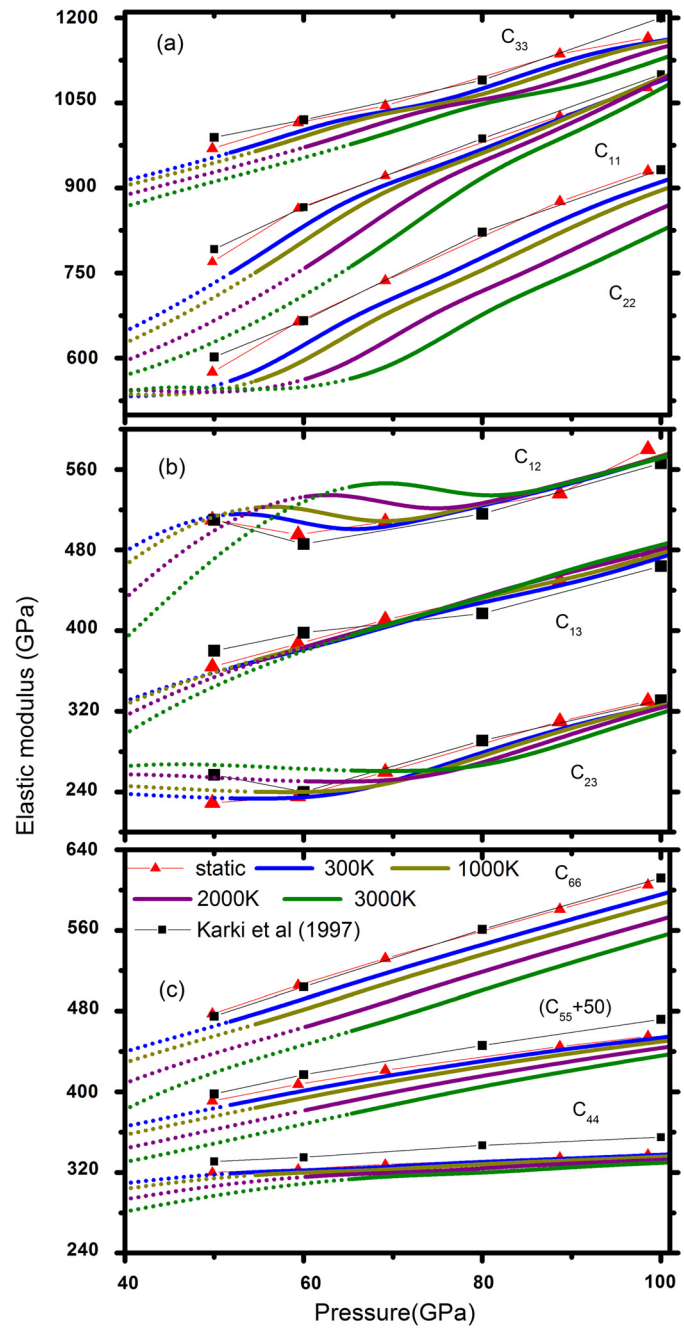

Fig. 2. Pressure dependence of elastic modulus of the $CaCl_2$-type silica at different temperatures, (a) C_{11}, C_{22} and C_{33}, (b) C_{12}, C_{13} and C_{23}, (c) C_{44}, C_{55} and C_{66}. Previous static calculation results reported by Karki et al. (1997b) are also listed. The results below the pressure of shear instability of stishovite are shown in the dotted lines.

3.2. Elastic wave velocity and anisotropy

Fig. 5 shows the pressure dependence of compressional (V_P) and shear (V_S) wave velocity in isotropic polycrystalline aggregates of stishovite and the $CaCl_2$-type silica at different temperatures.

Table 1
The elastic constants for polymorphs of silica.

	C_{11}	C_{22}	C_{33}	C_{12}	C_{13}	C_{23}	C_{44}	C_{55}	C_{66}
Stishovite at 0 GPa									
This study[a]	452		744	229	191		252		329
This study at 300K	431		722	200	183		243		312
Jiang et al. (2009)[b]	455		762	199	192		258		321
Brazhkin et al. (2005)[b]	466		775	207	204		258		310
Brazhkin et al. (2002)[b]	463		757	205	203		252		298
Holm and Ahuja (1999)[a]	480		735	245	220		260		340
Weidner et al. (1982)[b]	453		776	211	203		252		302
Karki et al. (1997b)[a]	462		734	210	195		255		324
$CaCl_2$-type structure at 50 GPa									
This study[a]	770	576	969	510	228	373	341	320	477
Karki et al. (1997b)[a]	794	602	988	516	255	382	350	332	475

[a] Calculation results at static condition.
[b] Experimental results at ambient temperature and pressure.

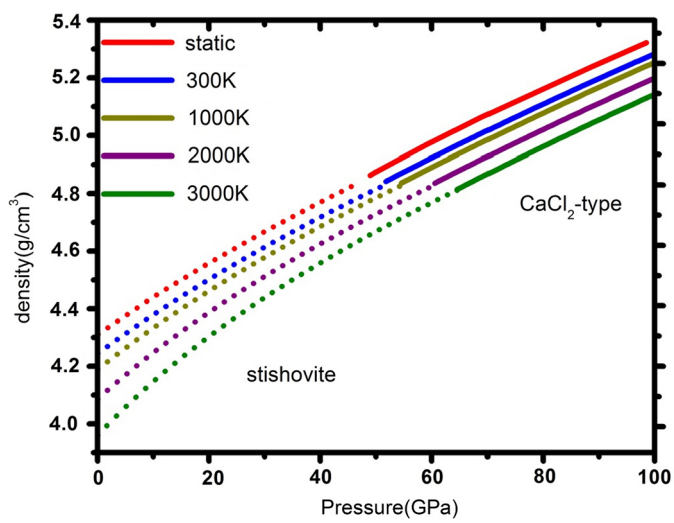

Fig. 3. Equation of states of the two polymorphs of silica at different temperatures. The dotted lines and the solid lines are the results for stishovite and the $CaCl_2$-type silica, respectively.

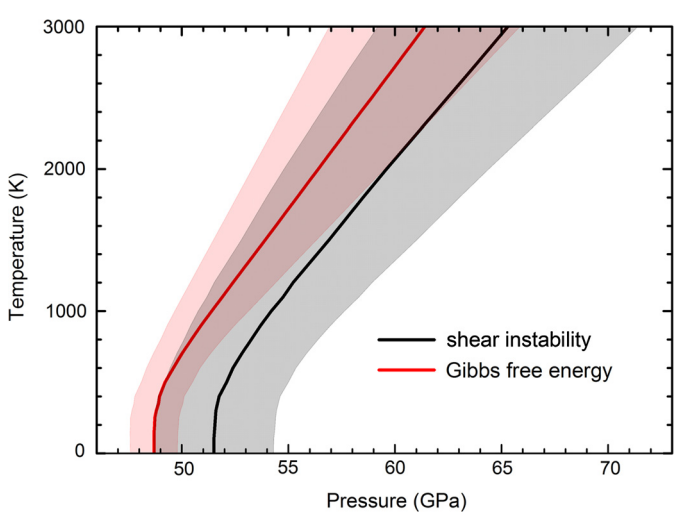

Fig. 4. Phase boundary based on shear instability and Gibbs free energy. The red shadow area shows the uncertainty in transition pressure based on Gibbs free energy, which was estimated from root mean square deviation of free energy when free energies versus volumes were fitted by isothermal third-order finite strain equations of state. The black shadow area shows the uncertainty in transition pressure based on shear instability, which was estimated from the root mean square deviation (∼1%) of the elastic constants C_{11} and C_{12}. (For interpretation of the references to color in this figure legend, the reader is referred to the web version of this article.)

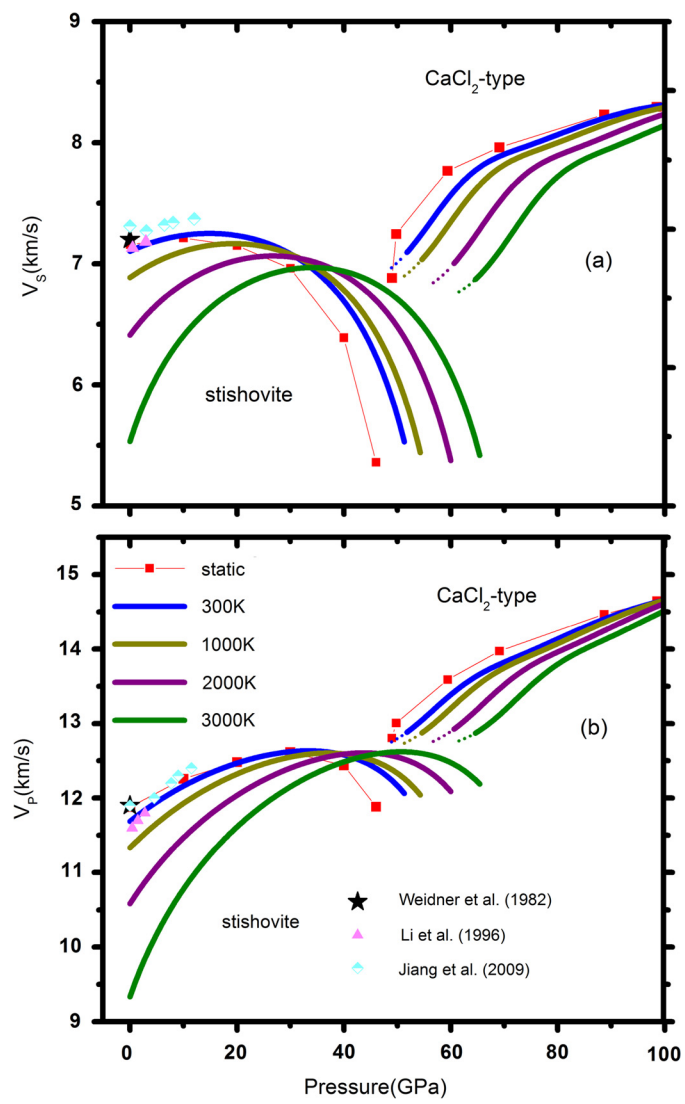

Fig. 5. (a) Shear wave velocities of and (b) P wave velocities of the two silicate polymorphs at different temperatures. All the velocities were calculated with VRH bounds. The dotted lines show the sound velocities of $CaCl_2$-type silica between transition pressure and pressure of stishovite's shear instability.

Because of the softening of the shear modulus, V_S of stishovite decreases with increasing pressure above certain pressure P_c. P_c increases with temperature because of the positive Clapeyron slope of the transition from stishovite to the $CaCl_2$-type silica, this makes V_S at different temperatures cross each other. At pressure larger

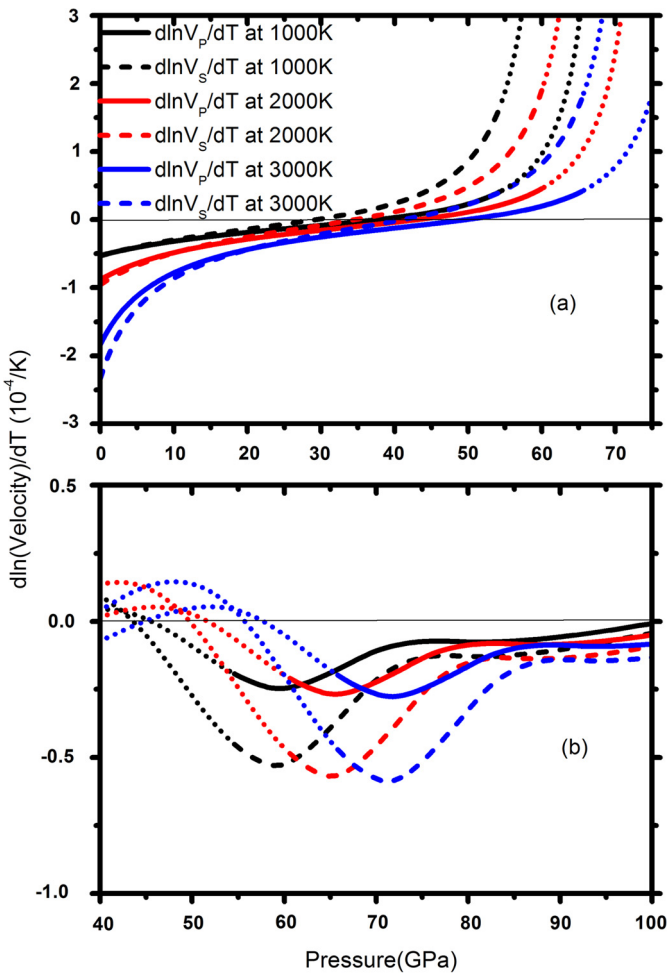

Fig. 6. $\frac{d\ln V_S}{dT}$ and $\frac{d\ln V_P}{dT}$ of (a) stishovite and of (b) the $CaCl_2$-type silica at different temperatures. The results beyond the stable pressure region of the two silicate polymorphs are shown in dotted lines.

than the crossover-point pressure, V_S of stishovite increases with increasing temperature, an unusual temperature-dependence feature. V_P of stishovite also exhibits the similar unusual behavior but this occurs at a higher pressure with a smaller temperature dependence (Fig. 6). Pressure can be divided into three regions based on the temperature dependence of V_P and V_S. Both V_P and V_S decrease with temperature in region I. V_P decreases while V_S increases with temperature in region II. Both V_P and V_S increase with temperature in region III. For the temperature range between 1000K and 2000K, region I < ~35 GPa, region II is at ~35–45 GPa and region III > ~45 GPa. Ferropericlase, one of the main minerals in the lower mantle, also shows the unusual temperature dependence but only in V_P not in V_S at the middle mantle depth (Wu et al., 2013). This is because spin crossover of iron causes dramatic softening in bulk modulus of ferropericlase. V_P of the lower mantle becomes insensitive to the temperature variation at around ~1750 km because significant increasing of V_P with temperature in ferropericlase cancels out the decreasing of V_P with temperature in silicate perovskite (Wu and Wentzcovitch, 2014). This may explain the disruption of plume image at 1500–2000 km depth below hotspots such as Hawaii and Iceland (Zhao, 2007) and worldwide disruption of V_P iso-surface representation structure at ~1700 km depth (van der Hilst and Karason, 1999). The $\frac{d\ln V_S}{dT}$ of stishovite increases quickly with pressure around phase boundary and reaches $\sim 1\times 10^{-4}$/K at phase boundary and -2×10^{-4}/K at shear instability boundary. These values are 3–7 times of the absolute value of the $\frac{d\ln V_S}{dT}$ of silicate perovskite, main composition of the lower mantle. Therefore, the unusual temperature dependence of V_P and V_S of stishovite may lead to some uncommon effects on lateral variation of V_P and V_S in slab region, where free silica is expected. In contrast to stishovite, the $CaCl_2$-type silica has normal temperature and pressure dependence in V_P and V_S. Both V_P and V_S increase with pressure while decrease with temperature.

The single crystal elastic wave velocities in different directions are determined by Christoffel equation (Musgrave, 1970)

$$\left|C_{ijkl}n_jn_l - \rho V^2\delta_{ik}\right| = 0 \tag{6}$$

where C_{ijkl} is the elastic constant tensor, $\mathbf{n} = (n_1, n_2, n_3)$ is a vector to show the propagation direction, ρ is the density, V is the velocity and ρV^2 is the eigenvalue of the 3×3 matrix. The corresponding eigenvector defines the polarization direction. Three eigenvalues of the matrix yield a quasi-compressional and two quasi-shear wave velocities for the propagation direction $\mathbf{n}$. The single crystal azimuthal anisotropies for P and S-waves are defined (Karki et al., 2001)

$$A_p = \frac{V_P^{max} - V_P^{min}}{V_P} \tag{7a}$$

$$A_s = \frac{V_S^{max} - V_S^{min}}{V_S} \tag{7b}$$

where V_P and V_S are the isotropic velocities. The difference in the velocities of the two shear waves (S1 and S2) propagating in a given direction leads to the polarization anisotropy. The maximum polarization anisotropy for the direction in which two shear velocities show the largest difference are defined as the polarization anisotropy

$$A_s{}^{po} = \frac{V_{S1} - V_{S2}}{V_S}. \tag{7c}$$

The stishovite at its whole stable pressure and temperature range exhibits a very strong elastic anisotropy especially for the shear wave velocities (Fig. 7) because of the softening of $C_{11} - C_{12}$. At pressure where $C_{11} - C_{12} = 0$, the shear velocity of stishovite propagating in [110]/[1$\bar{1}$0] with the polarization in [1$\bar{1}$0]/[110] decreases to 0, which results in the maximum of A_s and $A_s{}^{po}$. The maximum of A_s for the static result, 1.83, is in good consistence with the previous result (Karki et al., 2001). The maximum of $A_s{}^{po}$ is a little smaller than that of A_s. The temperature hardly changes the maximums but shifts the position of the maximums to the higher pressure. The anisotropy of the $CaCl_2$-type silica is also extremely strong, although A_s and $A_s{}^{po}$ drop dramatically about 0.5 when stishovite transforms into the $CaCl_2$-type silica. The maximum of the A_s of the $CaCl_2$-type silica (>0.8) is far larger than that of ferropericlase, a very anisotropic lower mantle mineral (Marquardt et al., 2009). A_p is much smaller than A_s and $A_s{}^{po}$ but is still large compared to most of the lower mantle minerals. At the phase boundary, the A_p of two polymorphs of silica is similar, which is fundamentally different from A_s and $A_s{}^{po}$.

4. Geophysical implications

Transition from stishovite to the $CaCl_2$-type silica has been used to explain the slab seismic discontinuity at the depth ~1200 km (~48 GPa) (e.g. Karki et al., 1997b; Niu, 2013; Tsuchiya, 2011; Vinnik et al., 2001) because the transition pressure based on most of the static first-principles calculations and room temperature experimental measurements is ~50 GPa. Considering the huge effect of temperature on transition pressure, however, the transition is most likely related to the seismic discontinuity far deeper than 1200 km (Fig. 8). Transition has a positive slope of ~5.0 ± 1.3 MPa/K and the transition depth is around 1400–1600 km

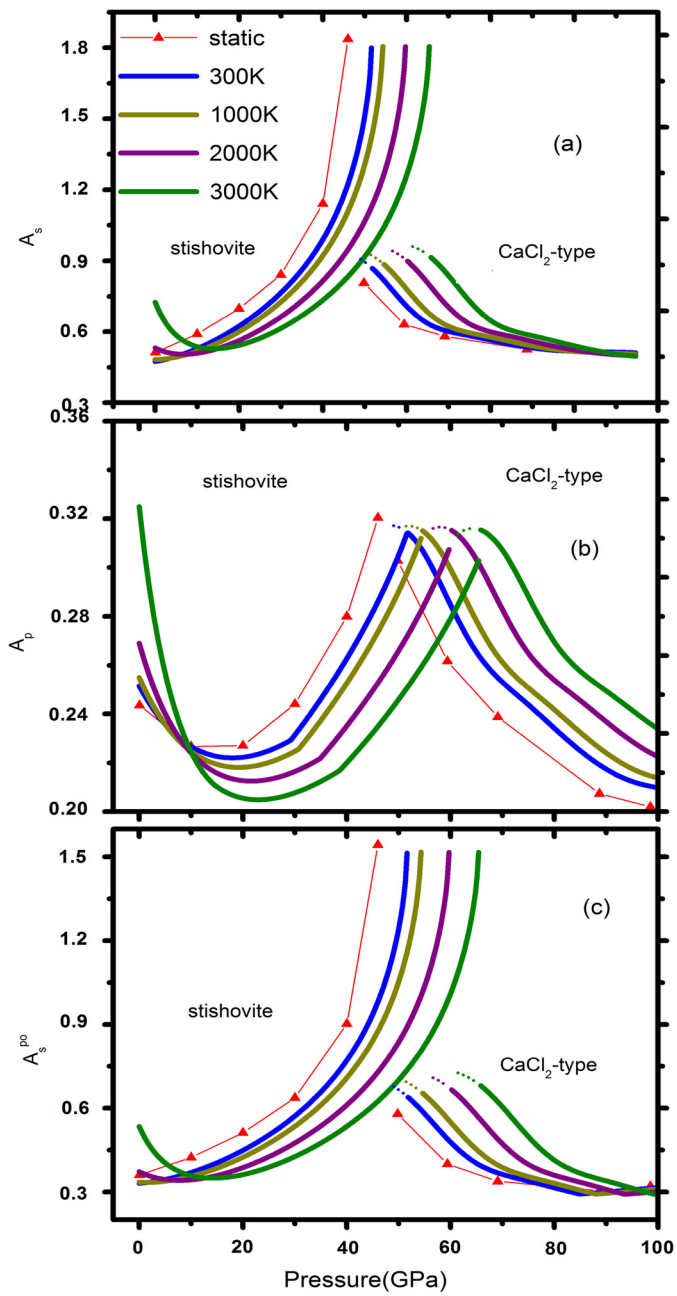

Fig. 7. The anisotropy, (a) A_s, (b) A_p, and (c) A_s^{po}, of stishovite and the $CaCl_2$-type silica at different temperatures. The dotted lines show anisotropy of $CaCl_2$-type silica between transition pressure and pressure of stishovite's shear instability.

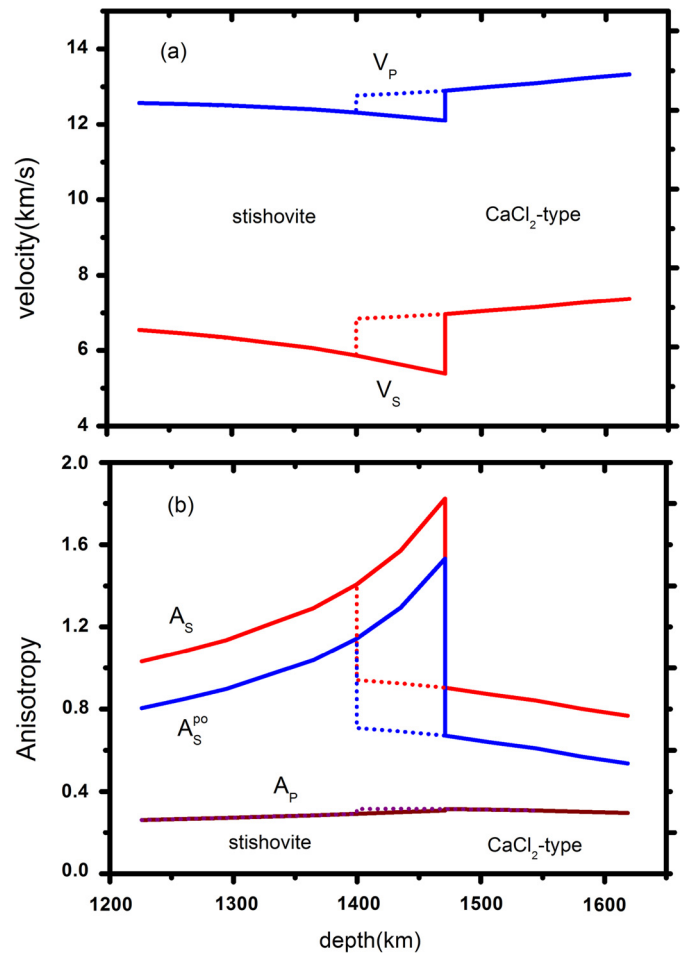

Fig. 8. (a) The velocities of V_S and V_P of silica along geotherm (Boehler, 2000), (b) the anisotropy of A_s, A_p, A_s^{po} of silica along geotherm (Boehler, 2000). All the velocities were calculated with VRH bounds. Discontinuities shown by solid lines and dotted lines correspond to the boundary based on shear instability and Gibbs free energy, respectively. $\Delta V_P = 0.8 \pm 0.15$ km/s, $\Delta V_S = 1.6 \pm 0.08$ km/s for solid lines, while $\Delta V_P = 0.45 \pm 0.15$ km/s, $\Delta V_S = 0.98 \pm 0.08$ km/s for dotted lines, where uncertainties were estimated based on the root mean square deviation (∼1%) of the elastic constants.

based on this and the previous calculation (Tsuchiya et al., 2004), which agrees within uncertainty with the transition depth of experimental measurement 1750 ± 250 km (Ono et al., 2002) and is also in consistence with usual underestimation of the transition pressure by LDA approximation (Yu et al., 2008). This calculation shows that the velocity jumps and anisotropy at phase boundary are almost independent of temperature. Because of the second order phase transition, the transition does not generate any density discontinuity but a velocity jump of $\sim 0.98 \pm 0.08$ km/s in V_S and $\sim 0.45 \pm 0.15$ km/s in V_P. If the transition is triggered by shear instability, velocity jump can be $\sim 1.6 \pm 0.08$ km/s in V_S and $\sim 0.8 \pm 0.15$ km/s in V_P (Fig. 8). Transition from stishovite to the $CaCl_2$-type silica may be related to the seismic discontinuity at a depth of about 1670 km in the vicinity of Mariana Island (Kaneshima and Helffrich, 1998, 1999; Vinnik et al., 2001). Kaneshima and Helffrich (1998) attributed the discontinuity to a subducted slab. Observed seismic discontinuity with V_S around 0.3 km/s (Vinnik et al., 2001) can be produced by an aggregation with 20–30% free silica. This percentage of free silica is possible at the region associated with subduction. Petrologic studies of the mid-ocean-ridge basalt (MORB) show that at the lower mantle condition, MORB can possess 10–20% free silica (Irifune and Ringwood, 1993; Kesson et al., 1994; Ono et al., 2001). The anisotropy of stishovite is so strong that even a few percent may cause a considerable seismic anisotropy (Fig. 8). We may expect the observable seismic anisotropy at depth ∼1670 km in the vicinity of Mariana Island where seismic discontinuity has been observed. V_S of stishovite increases unusually with temperature around the phase boundary. The $\frac{d \ln V_S}{dT}$ at phase boundary, is 3–7 times of the absolute value of the $\frac{d \ln V_S}{dT}$ of silicate perovskite. Therefore V_S for the aggregation with 20–30% stishovite will become temperature insensitive or even increase slight with temperature around the phase boundary. This may result in some observable effects on lateral variation of V_S.

5. Conclusion

Because of the softening of the shear modulus at high pressure, stishovite at high pressure is known as one of the most anisotropic

silicates. The maximum of the azimuthal anisotropy for S-waves and polarization anisotropy, which occurs just before stishovite experiences the shear instability, is far larger than 1. The transition from stishovite to $CaCl_2$-type silica is accompanied by a jump of $\sim 0.98 \pm 0.08$ km/s in V_S and $\sim 0.45 \pm 0.15$ km/s in V_P. The Clapeyron slope of the transition is positive, $\sim 5.0 \pm 1.3$ MPa/K. Due to the softening of the shear modulus and the positive Clapeyron slope of the shear instability, sound velocities at different temperatures cross each other. This leads to the unusual positive temperature dependence of sound velocities around phase transition boundary. The temperature dependences of sound velocities depend on the pressure. At the relatively low pressure, both V_P and V_S decrease with temperature. In narrow pressure region around 40 GPa, V_P decreases while V_S increases with temperature. At the higher pressure, both V_P and V_S increase with temperature. Transition from stishovite to the $CaCl_2$-type silica at lower mantle's temperature occurs at depth far deeper than 1200 km. This transition is most likely related to the seismic discontinuity at depth $\sim$1670 km in a vicinity of Mariana Island. The estimated amount of free silica in the aggregation to produce 0.3 km/s V_S discontinuity is about 20–30%. With large and unusual positive temperature dependence of V_S and strong anisotropy of stishovite around phase boundary, we may expect some uncommon effects on lateral variations of V_S and observable seismic anisotropy around the seismic discontinuity region.

Acknowledgements

This work is supported by State Key Development Program of Basic Research of China (2014CB845905), the Fundamental Research Funds for the Central Universities (WK2080000040), the National Natural Science Foundation of China (41274087), Chinese Academy of Sciences International Partnership Program for Creative Research Teams. The calculations were conducted in the Shanghai supercomputer center.

References

Andrault, D., Angel, R.J., Mosenfelder, J.L., Le Bihan, T., 2003. Equation of state of stishovite to lower mantle pressures. Am. Mineral. 88, 301–307.

Andrault, D., Fiquet, G., Guyot, F., Hanfland, M., 1998. Pressure-induced Landau-type transition in stishovite. Science 282, 720–724.

Asahara, Y., Hirose, K., Ohishi, Y., Hirao, N., Ozawa, H., Murakami, M., 2013. Acoustic velocity measurements for stishovite across the post-stishovite phase transition under deviatoric stress: implications for the seismic features of subducting slabs in the mid-mantle. Am. Mineral. 98, 2053–2062.

Baroni, S., de Gironcoli, S., Dal Corso, A., Giannozzi, P., 2001. Phonons and related crystal properties from density-functional perturbation theory. Rev. Mod. Phys. 73, 515–562.

Barron, T.H.K., Klein, M.L., 1965. Second-order elastic constants of a solid under stress. Proc. Phys. Soc. Lond. 85, 523–532.

Belonoshko, A.B., Dubrovinsky, L.S., 1996. Molecular and lattice dynamics study of the MgO–SiO_2 system using a transferable interatomic potential. Geochim. Cosmochim. Acta 60, 1645–1656.

Boehler, R., 2000. High-pressure experiments and the phase diagram of lower mantle and core materials. Rev. Geophys. 38, 221–245.

Brazhkin, V.V., Grimsditch, M., Gue des, I., Bendeliani, N.A., Dyuzheva, T.I., Lityagina, L.M., 2002. Elastic moduli and the mechanical properties of stishovite single crystals. Phys. Uspekhi 45, 447–448.

Brazhkin, V.V., McNeil, L.E., Grimsditch, M., Bendeliani, N.A., Dyuzheva, T.I., Lityagina, L.M., 2005. Elastic constants of stishovite up to its amorphization temperature. J. Phys.: Condens. Matter 17, 1869–1875.

Carpenter, M.A., 2006. Elastic properties of minerals and the influence of phase transitions. Am. Mineral. 91, 229–246.

Carpenter, M.A., Hemley, R.J., Mao, H.K., 2000. High-pressure elasticity of stishovite and the $P42/mnm \rightleftharpoons Pnnm$ phase transition. J. Geophys. Res. 105, 10807–10816.

Cohen, R.E., 1991. Bonding and elasticity of stishovite SiO_2 at high-pressure – linearized augmented plane-wave calculations. Am. Mineral. 76, 733–742.

Cohen, R.E., 1992. First-principles predictions of elasticity and phase transitions in high pressure SiO_2 and geophysical implications. In: High-Pressure Research: Application to Earth and Planetary Sciences. American Geophysical Union, pp. 425–431.

Driver, K.P., Cohen, R.E., Wu, Z.G., Militzer, B., Rios, P.L., Towler, M.D., Needs, R.J., Wilkins, J.W., 2010. Quantum Monte Carlo computations of phase stability, equations of state, and elasticity of high-pressure silica. Proc. Natl. Acad. Sci. USA 107, 9519–9524.

Dubrovinsky, L.S., Belonoshko, A.B., 1996. Pressure-induced phase transition and structural changes under deviatoric stress of stishovite to $CaCl_2$-like structure. Geochim. Cosmochim. Acta 60, 3657–3663.

Giannozzi, P., Baroni, S., Bonini, N., Calandra, M., Car, R., Cavazzoni, C., Ceresoli, D., Chiarotti, G.L., Cococcioni, M., Dabo, I., Dal Corso, A., de Gironcoli, S., Fabris, S., Fratesi, G., Gebauer, R., Gerstmann, U., Gougoussis, C., Kokalj, A., Lazzeri, M., Martin-Samos, L., Marzari, N., Mauri, F., Mazzarello, R., Paolini, S., Pasquarello, A., Paulatto, L., Sbraccia, C., Scandolo, S., Sclauzero, G., Seitsonen, A.P., Smogunov, A., Umari, P., Wentzcovitch, R.M., 2009. Quantum espresso: a modular and open-source software project for quantum simulations of materials. J. Phys.: Condens. Matter 21, 19.

Hemley, R.J., Shu, J., Carpenter, M.A., Hu, J., Mao, H.K., Kingma, K.J., 2000. Strain/order parameter coupling in the ferroelastic transition in dense SiO_2. Solid State Commun. 114, 527–532.

Holm, B., Ahuja, R., 1999. Ab initio calculation of elastic constants of SiO_2 stishovite and alpha-quartz. J. Chem. Phys. 111, 2071–2074.

Irifune, T., Ringwood, A.E., 1993. Phase transformations in subducted oceanic crust and buoyancy relationships at depths of 600–800 km in the mantle. Earth Planet. Sci. Lett. 117, 101–110.

Jiang, F., Gwanmesia, G.D., Dyuzheva, T.I., Duffy, T.S., 2009. Elasticity of stishovite and acoustic mode softening under high pressure by Brillouin scattering. Phys. Earth Planet. Inter. 172, 235–240.

Kaneshima, S., Helffrich, G., 1998. Detection of lower mantle scatterers northeast of the Marianna subduction zone using short-period array data. J. Geophys. Res. 103, 4825–4838.

Kaneshima, S., Helffrich, G., 1999. Dipping low-velocity layer in the mid-lower mantle: evidence for geochemical heterogeneity. Science 283, 1888–1892.

Karki, B.B., Warren, M.C., Stixrude, L., Ackland, G.J., Crain, J., 1997a. Ab initio studies of high-pressure structural transformations in silica. Phys. Rev. B 55, 3465–3471.

Karki, B.B., Stixrude, L., Crain, J., 1997b. Ab initio elasticity of three high-pressure polymorphs of silica. Geophys. Res. Lett. 24, 3269–3272.

Karki, B.B., Stixrude, L., Wentzcovitch, R.M., 2001. High-pressure elastic properties of major materials of Earth's mantle from first principles. Rev. Geophys. 39, 507–534.

Kesson, S.E., Fitz Gerald, J.D., Shelley, J.M.G., 1994. Mineral chemistry and density subducted basaltic crust at lower-mantle pressures. Nature 372, 767–769.

Kingma, K.J., Cohen, R.E., Hemley, R.J., Mao, H.K., 1995. Transformation of stishovite to a denser phase at lower-mantle pressures. Nature 374, 243–245.

Kohn, W., Sham, L.J., 1965. Self-consistent equations including exchange and correlation effects. Phys. Rev. 140, 1133.

Lee, C., Gonze, X., 1995. Ab initio calculation of the thermodynamic properties and atomic temperature factors of SiO_2 α-quartz and stishovite. Phys. Rev. B 51, 8610.

Lee, C., Gonze, X., 1997. SiO_2 stishovite under high pressure: dielectric and dynamical properties and the ferroelastic phase transition. Phys. Rev. B 56, 7321.

Li, B., Rigden, S.M., Liebermann, R.C., 1996. Elasticity of stishovite at high pressure. Phys. Earth Planet. Inter. 96, 113–127.

Marquardt, H., Speziale, S., Reichmann, H.J., Frost, D.J., Schilling, F.R., Garnero, E.J., 2009. Elastic shear anisotropy of ferropericlase in Earth's lower mantle. Science 324, 224–226.

Monkhorst, H.J., Pack, J.D., 1976. Special points for Brillouin-zone integrations. Phys. Rev. B 13, 5188–5192.

Musgrave, M.J.P., 1970. Crystal Acoustics. Holden-Day, Boca Raton, FL.

Niu, F., 2013. Distinct compositional thin layers at mid-mantle depths beneath northeast China revealed by the USArray. Earth Planet. Sci. Lett. http://dx.doi.org/10.1016/j.epsl.2013.02.015.

Núñez Valdez, M., Umemoto, K., Wentzcovitch, R.M., 2012a. Elasticity of diamond at high pressures and temperatures. Appl. Phys. Lett. 101, 171902.

Núñez Valdez, M., Wu, Z., Yu, Y.G., Wentzcovitch, R.M., 2012b. Thermoelastic properties of ringwoodite $(Fe_x, Mg_{1-x})_2SiO_4$: its relationship to the 520 km seismic discontinuity. Earth Planet. Sci. Lett. 351–352, 115–122.

Núñez Valdez, M., Wu, Z., Yu, Y., Wentzcovitch, R., 2013. Thermal elasticity of $(Fe_x, Mg_{1-x})_2SiO_4$ olivine and wadsleyite. Geophys. Res. Lett. 40, 290–294.

Ono, S., Hirose, K., Murakami, M., Isshiki, M., 2002. Post-stishovite phase boundary in SiO_2 determined by in situ X-ray observations. Earth Planet. Sci. Lett. 197, 187–192.

Ono, S., Ito, E., Katsura, T., 2001. Mineralogy of subducted basaltic crust (MORB) from 25 to 37 GPa, and chemical heterogeneity of the lower mantle. Earth Planet. Sci. Lett. 190, 57–63.

Shieh, S.R., Duffy, T.S., Li, B., 2002. Strength and elasticity of SiO_2 across the stishovite–$CaCl_2$-type structural phase boundary. Phys. Rev. Lett. 89, 255507.

Togo, A., Oba, F., Tanaka, I., 2008. First-principles calculations of the ferroelastic transition between rutile-type and $CaCl_2$-type SiO_2 at high pressures. Phys. Rev. B 78, 134106.

Troullier, N., Martins, J.L., 1991. Efficient pseudopotentials for plane-wave calculations. Phys. Rev. B 43, 1993–2006.
Tsuchida, Y., Yagi, T., 1989. A new, post-stishovite high-pressure polymorph of silica. Nature 340, 217–220.
Tsuchiya, T., 2011. Elasticity of subducted basaltic crust at the lower mantle pressures: insights on the nature of deep mantle heterogeneity. Phys. Earth Planet. Inter. 188, 142–149.
Tsuchiya, T., Caracas, R., Tsuchiya, J., 2004. First principles determination of the phase boundaries of high-pressure polymorphs of silica. Geophys. Res. Lett. 31, L11610.
Tsuneyuki, S., Matsui, Y., Aoki, H., Tsukada, M., 1989. New pressure-induced structural transformations in silica obtained by computer-simulation. Nature 339, 209–211.
van der Hilst, R.D., Karason, H., 1999. Compositional heterogeneity in the bottom 1000 kilometers of Earth's mantle: toward a hybrid convection model. Science 283, 1885–1888.
Vinnik, L., Kato, M., Kawakatsu, H., 2001. Search for seismic discontinuities in the lower mantle. Geophys. J. Int. 147, 41–56.
Weidner, D.J., Bass, J.D., Ringwood, A.E., Sinclair, W., 1982. The single-crystal elastic-moduli of stishovite. J. Geophys. Res. 87, 4740–4746.
Wentzcovitch, R.M., Martins, J.L., Price, G., 1993. Ab initio molecular dynamics with variable cell shape: application to $MgSiO_3$. Phys. Rev. Lett. 70, 3947.
Wu, Z., 2010. Calculating the anharmonic free energy from first principles. Phys. Rev. B 81, 172301.
Wu, Z., Wentzcovitch, R.M., 2009. Effective semiempirical ansatz for computing anharmonic free energies. Phys. Rev. B 79, 104304.
Wu, Z., Wentzcovitch, R.M., 2011. Quasiharmonic thermal elasticity of crystals: an analytical approach. Phys. Rev. B 83, 8.
Wu, Z., Wentzcovitch, R.M., 2014. Spin crossover inferropericlase and velocity heterogeneities in the lower mantle. Proc. Natl. Acad. Sci. USA. www.pnas.org/cgi/doi/10.1073/pnas.1322427111.
Wu, Z., Justo, J.F., Wentzcovitch, R.M., 2013. Elastic anomalies in a spin-crossover system: ferropericlase at lower mantle conditions. Phys. Rev. Lett. 110, 228501.
Yu, Y.G.G., Wu, Z., Wentzcovitch, R.M., 2008. Alpha–beta–gamma transformations in Mg_2SiO_4 in Earth's transition zone. Earth Planet. Sci. Lett. 273, 115–122.
Zha, C.-s., Hemley, R.J., Mao, H.-k., Duffy, T.S., Meade, C., 1994. Acoustic velocities and refractive index of SiO_2 glass to 57.5 GPa by Brillouin scattering. Phys. Rev. B 50, 13105.
Zhao, D.P., 2007. Seismic images under 60 hotspots: search for mantle plumes. Gondwana Res. 12, 335–355.